High-Frequency Effect Due to the Axial Drift Velocity of a Plasma Column

A. M. MESSIAEN*
Laboratoire de Physique, Centre des Sciences Nucléaires, Ecole Royale Militaire, Bruxelles, Belgium

AND

P. E. VANDENPLAS†
California Institute of Technology, Pasadena, California

(Received 20 September 1965)

The scattering of a plane electromagnetic wave with normal incidence (**E** field perpendicular to the axis) by a plasma column in the presence of a static magnetic induction $\mathbf{B}_0$ has been studied earlier. A heretofore unexplained effect, however, is the existence of a scattered axial field E_Z even when $B_0=0$. A mechanism responsible for this coupling between the E_Z and the transverse **E** field, in the absence of B_0, is investigated here, namely the role of an axial drift velocity v_d. The effect observed is a resonance peak of E_Z occurring at the same density for which there exists a resonance of the scattered transverse **E** field which is well explained by a uniform cold-plasma model. The same model is therefore assumed here. In this approximation the plasma can be described by a surface charge density Σ due to the HF polarization which gives rise to a surface current density $\mathbf{K}=\Sigma\mathbf{v}_d$. The boundary conditions then lead to the existence of an E_Z which, for $B_0=0$, has a $\sin\theta$ dependence when the exciting field has a $\cos\theta$ dependence. When $B_0\neq 0$, a more complicated theoretical spectrum is obtained. Both the position and the angular dependence of the resonances are in very good agreement with experimental data. The effect predicted by this model is, however, more than an order of magnitude below that observed in a mercury plasma column. This phenomenon can be described as the plasma radio-frequency analog of the static field induced by the Roentgen-Eichenwald current.

1. INTRODUCTION

THE scattering of an electromagnetic wave by a cylinder of plasma has been extensively studied recently. An interesting resonance pattern is observable in the absence of a static magnetic field[1–7] or in the presence of a static magnetic induction $\mathbf{B}_0$.[2,4,8] In the absence of $\mathbf{B}_0$ the main resonance or the two (or four) main resonances of a hollow plasma cylinder[9] are very well explained by the cold plasma approach (electron temperature T_e equal to zero). The secondary resonances are precisely explained by the nonzero temperature of a nonuniform plasma, including the fact that there exists no series limit for these resonances.[7,10,11] A variation principle has been given for estimating the eigenfrequencies of a finite warm nonuniform plasma in an arbitrary electric or magnetic field.[12] Finally, the effect of stronger magnetic fields on temperature resonances have received detailed attention lately.[13,14]

The positions of the electric vector $\mathbf{E}_{\text{inc}}$, the magnetic induction vector $\mathbf{B}_{\text{inc}}$, and the Poynting vector $\mathbf{S}_{\text{inc}}$ of the incoming wave are indicated in Fig. 1. The components of the scattered field $\mathbf{E}_{\text{sc}}$ are indicated in the cylindrical coordinate system r, θ, Z. In a former work we studied, in the cold plasma approximation, the influence of the anisotropy and the inhomogeneity arising from a static magnetic induction $\mathbf{B}_0$ on the resonance spectrum of the scattered wave, and these theoretical results were compared with experimental data.[15,16] One of the observed effects remained unexplained, however, and that is the existence of an $E_{Z\text{sc}}$ component[16b] even in the absence of $\mathbf{B}_0$. We will now

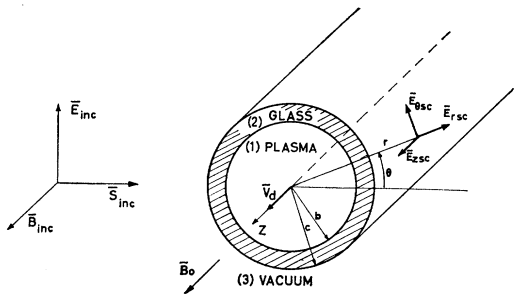

FIG. 1. Incoming plane wave and scattered wave with respect to the plasma characterized by a drift velocity v_d.

* Chercheur agréé de l'Institut Interuniversitaire des Sciences Nucléaires.

† On leave of absence from the Ecole Royale Militaire, Bruxelles, Belgium.

[1] D. Romell, Nature **167**, 243 (1951).
[2] A. Dattner, Ericsson Tech. **2**, 309 (1957); **8**, 1 (1963).
[3] G. D. Boyd, L. M. Field, and R. W. Gould, Phys. Rev. **109**, 1393 (L) (1958).
[4] A. M. Messiaen and P. E. Vandenplas, Physica **28**, 537 (1962) and **30**, 2309 (1964).
[5] G. Bryant and N. Franklin, Proc. Phys. Soc. **81**, 531 (1963).
[6] F. W. Crawford, J. Appl. Phys. **35**, 1365 (1964).
[7] J. V. Parker, J. C. Nickel, and R. W. Gould, Phys. Fluids **7**, 1489 (1964).
[8] F. W. Crawford, G. S. Kino, and A. B. Cannara, J. Appl. Phys. **34**, 3168, (1963).
[9] (a) A. M. Messiaen and P. E. Vandenplas, J. Nucl. Energy Pt. C **4**, 267 (1962); (b) P. E. Vandenplas and A. M. Messiaen, *ibid.* **6**, 71 (1964).
[10] P. E. Vandenplas and R. W. Gould, Nucl. Fusion Suppl. **3**, 1155 (1962). J. Nucl. Energy Pt. C **6**, 449 (1964) and P. E. Vandenplas and A. M. Messiaen, *ibid.* **6**, 459 (1964).
[11] P. Weissglas, J. Nucl. Energy Pt. C **6**, 251 (1964).
[12] E. M. Barston, Phys. Rev. **139**, A394 (1965).
[13] S. J. Buchsbaum and A. Hasegawa, Phys. Letters **12**, 685 (1964); Phys. Rev. **143**, 303 (1966).
[14] H. J. Schmitt, G. Meltz, and P. J. Freyheit, Phys. Rev. **139**, A1432 (1965).
[15] A. M. Messiaen and P. E. Vandenplas, Phys. Letters **2**, 193 (1962).
[16] (a) P. E. Vandenplas and A. M. Messiaen, Nucl. Fusion **5**, 47 (1965); (b) A. M. Messiaen and P. E. Vandenplas, *ibid.* **5**, 56 (1965).

study a mechanism responsible for the coupling between the cross-polarized **E** mode (**E**⊥axis), which is the only one excited, and the cross-polarized **H** mode (**H**⊥axis) in the absence of $\mathbf{B}_0$ and see how an axial $\mathbf{B}_0$ enhances this coupling.

When $\mathbf{B}_0=0$, the effect observed is the existence of a resonance peak of $\mathbf{E}_{Zsc}$ at the same electron plasma density $\langle N_e\rangle$ as that for which the main resonance of the TE mode occurs. This last resonance is well explained by cold-plasma theory of a uniform column. We will therefore assume $T_e=0$ and a constant $\langle N_e\rangle$ in the column as formerly.[15,16(a)] The new feature is that one takes into account the fact that the plasma possesses an axial drift velocity $\mathbf{v}_d=v_d\mathbf{1}_z$ ($\mathbf{1}_z$: unit vector along the Z axis) as it is generated in the positive column of a low-pressure Hg discharge. The plasma can then be described theoretically by a surface charge density of high-frequency polarization which, because of the drift velocity $\mathbf{v}_d$, gives rise to the existence of a scattered $\mathbf{E}_{Zsc}$ which, for $\mathbf{B}_0=0$, has an angular dependence in $\sin n\theta$ when the excitation by the incoming field is in $\cos n\theta$ for $\mathbf{E}_\theta$. This $\mathbf{E}_{Zsc}$ displays a resonance for the expected value of $\langle N_e\rangle$. When $\mathbf{B}_0=B_0\mathbf{1}_z\neq 0$, one obtains theoretically a more complicated spectrum which is also in good agreement with the experimental data.

It is very interesting to note that this phenomenon can be considered as the plasma high-frequency analog of the static field induced by the Roentgen-Eichenwald current[17–19] as is pointed out in the conclusions.

It must be stressed that the agreement between theory and experiment is excellent concerning the position and the θ dependence of the resonances, but that the amplitude of the effect predicted for the cold uniform plasma is at least one order of magnitude below the effect observed with the mercury plasma column.

The fact that the drift velocity $\mathbf{v}_d$ of a plasma gives rise to an electromagnetic field with **E** parallel to $\mathbf{v}_d$ when an electromagnetic field exists with **E** perpendicular to $\mathbf{v}_d$, and that this coupling is further complicated and enhanced by the presence of a static magnetic field, is a feature of general interest. Such an effect can be important and should be taken into account in several plasma set-ups.

A summary of the present work has already been given.[20]

2. THEORY

A. General Equations

We consider a collisionless cold plasma ($T_e=0$) with constant electron equilibrium density $\langle N_e\rangle$. Because of translational symmetry along the Z axis, the problem is characterized by $\partial/\partial Z\equiv 0$. The linearized hydrodynamical equation for the transport of momentum of the electrons is

$$-i\omega\mathbf{u}+(\mathbf{v}_d\cdot\nabla)\mathbf{u} =-(e/m)[\mathbf{E}+\mathbf{v}_d\times\mathbf{B}+\mathbf{u}\times\mathbf{B}_{0T}]-en\mathbf{E}_0/m\langle N_e\rangle, \quad (1)$$

where **u** is the average perturbed electron velocity, **E** and **B** are the perturbed electric and magnetic induction fields in the plasma. The time dependence of the perturbed quantities is in $e^{-i\omega t}$. The charge and mass of the electrons are noted $-e$ and m. The introduction of $\partial/\partial Z\equiv 0$ in (1) imposes $(\mathbf{v}_d\cdot\nabla)\mathbf{u}=0$. Furthermore, the term $\mathbf{v}_d\times\mathbf{B}$ can be neglected. Indeed when $\mathbf{v}_d=0$, **B** is parallel to $\mathbf{v}_d$ and this term is exactly zero; when $\mathbf{v}_d\neq 0$ this term can be neglected in first approximation because it is a second-order effect as the transverse part of **B** is of order E_{Zsc}/c.

$\mathbf{B}_{0T}$ is the total static magnetic induction resulting from the applied axial $\mathbf{B}_0$ and from the $B_{0\theta}$ due to the static discharge current density $\mathbf{J}_0$. Neglecting the ionic contribution, we have $\mathbf{J}_0=-e\langle N_e\rangle\mathbf{v}_d$ and $B_{0\theta}=\mu_0 J_0 r/2$. The effect of this $B_{0\theta}$ field is studied in Appendix A where it is shown that it can be neglected to the order of the approximations used in this paper. We shall therefore only consider the effect of the applied axial $\mathbf{B}_0$. The field $\mathbf{E}_0=E_0\mathbf{1}_Z$, where $\mathbf{1}_Z$ is the unit vector in the Z direction, is the axial electrostatic field which is linked to $\mathbf{v}_d$ by the electron mobility μ_e such that $\mathbf{v}_d=\mu_e\mathbf{E}_0$; n is the perturbed electron density.

Equation (1) is then written as

$$-e\langle N_e\rangle\mathbf{u}=\boldsymbol{\sigma}\cdot\mathbf{E}-e^2 n\mathbf{v}_d/i\omega m\mu_e, \quad (2)$$

with

$$\boldsymbol{\sigma}=\frac{\epsilon_0\omega_e^2}{+i\omega}\begin{bmatrix}-\dfrac{1}{1-\beta^2} & i\dfrac{\beta}{1-\beta^2} & 0\\ -i\dfrac{\beta}{1-\beta^2} & -\dfrac{1}{1-\beta^2} & 0\\ 0 & 0 & -1\end{bmatrix},$$

$$\omega_e^2=\frac{e^2\langle N_e\rangle}{m\epsilon_0};\quad \beta=\frac{eB_0}{m\omega}.$$

$\boldsymbol{\sigma}$ is defined as the high-frequency tensorial conductivity of the plasma and is independent of v_d. Hence the perturbed plasma current density is

$$\mathbf{J}=-e(\langle N_e\rangle\mathbf{u}+n\mathbf{v}_d)=\boldsymbol{\sigma}\cdot\mathbf{E}-en\mathbf{v}_d\left(1+\frac{e}{i\omega m\mu_e}\right). \quad (3)$$

Since $\mu_e\cong 5\times 10^3 m^2\,\mathrm{sec}^{-1}\,\mathrm{V}^{-1}$ in typical experiments with mercury, $e^2/i\omega m\mu_e\cong 1.9\times 10^{-3}$ (when $\omega/2\pi=2.7$ GHz) and can be neglected right away. The plasma is

[17] W. C. Roentgen, Ann. Phys. **35**, 264 (1888) and **40**, 93 (1890).
[18] A. Eichenwald, Ann. Phys. **11**, 421 (1903).
[19] A. Sommerfeld, *Electrodynamics* (Academic Press Inc., New York, 1952), pp. 283–285.
[20] P. E. Vandenplas and A. M. Messiaen, Bull. Am. Phys. Soc. **11**, 577 (1966); A. M. Messiaen and P. E. Vandenplas, Phys. Letters **20**, 14 (1966).

described by (2) and (3) and by Maxwell's equations:

$$\text{curl}\mathbf{H}=\mathbf{J}-i\omega\epsilon_0\mathbf{E}, \tag{4}$$

$$\text{div}\mathbf{E}=-en/\epsilon_0, \tag{5}$$

$$\text{curl}\mathbf{E}=i\omega\mu_0\mathbf{H}, \tag{6}$$

$$\text{div}\mathbf{H}=0. \tag{7}$$

The perturbed density n can be expressed as a function of $\mathbf{J}$, given by (3), through the continuity equation; we obtain

$$-en=\frac{\epsilon_0\omega_e^2}{\omega^2}\left(\frac{1}{1-\beta^2}\,\text{div}\mathbf{E}-\frac{i\beta}{1-\beta^2}\,\text{curl}_Z\mathbf{E}\right)-\frac{e\,\text{div}(n\mathbf{v}_d)}{i\omega}. \tag{8}$$

One has $\text{div}(n\mathbf{v}_d)=n\,\text{div}\mathbf{v}_d+\mathbf{v}_d\cdot\text{grad}n=0$ as $\partial/\partial Z\equiv 0$.

Let us first examine this equation in the absence of the static magnetic field ($\beta=0$). Using (5) one finds the classic result $n=0$ in the bulk of the plasma when $\omega\neq\omega_e$. This means that there will be a perturbed surface density and that the surface phenomena will be extremely important in this description.

When $\beta\neq 0$, the result $n=0$ in the bulk of the plasma no longer holds and we have a perturbed density given by

$$e\left[1-\frac{\omega_e^2}{\omega^2(1-\beta^2)}\right]n=\frac{i\beta}{1-\beta^2}\frac{\epsilon_0\omega_e^2}{\omega^2}\,\text{curl}_Z\mathbf{E}.$$

For $\beta\ll 1$ we may neglect this bulk density perturbation with respect to the perturbed surface density in the expression of $\mathbf{J}$ as given by (3) because the ratio of the bulk drift current to the surface drift current is of the order of $\beta b/\lambda_0$ ($b/\lambda_0\ll 1$ in this problem). We therefore assume that there is no bulk density perturbation.

B. Surface Equations

The plasma is connected to the neighboring medium through Maxwell's surface equations

$$\text{curl}_s\mathbf{H}=\mathbf{K}, \tag{9}$$

$$\text{div}_s\mathbf{D}=\Sigma, \tag{10}$$

$$\text{curl}_s\mathbf{E}=0, \tag{11}$$

$$\text{div}_s\mathbf{H}=0, \tag{12}$$

and the surface continuity equation

$$-i\omega\Sigma+\text{div}_s\mathbf{J}=0, \tag{13}$$

where Σ is the surface charge density and $\mathbf{K}$ the surface current density. We must now establish the expressions of these two quantities as a function of plasma properties. As the medium 2 surrounding the plasma (medium 1) is a dielectric (see Fig. 1), Eq. (13) becomes

$$(J_{1r})_{r=b}=[(\boldsymbol{\sigma}\cdot\mathbf{E}_1)\cdot\mathbf{1}_r]_{r=b}=-i\omega\Sigma, \tag{14}$$

where $\mathbf{1}_r$ is the unit vector along r. Let us note that (10) can then be written as

$$(\epsilon_2 E_{2r})_{r=b}=\left[\left(\left(\epsilon_0-\frac{\boldsymbol{\sigma}}{i\omega}\right)\cdot\mathbf{E}_1\right)\cdot\mathbf{1}_r\right]_{r=b}=[(\boldsymbol{\epsilon}_p\cdot\mathbf{E}_1)\cdot\mathbf{1}_r]_{r=b}, \tag{15}$$

where $\boldsymbol{\epsilon}_p$ is the standard equivalent tensorial permittivity. To obtain $\mathbf{K}$ we must consider the surface limit of (3), taking into account that $-en=\Sigma\,\delta(r-b)$, where δ is the delta function. This leads to $\mathbf{K}=\Sigma\,\mathbf{v}_d$ and means that the plasma is described as moving as a whole with velocity $\mathbf{v}_d$; the applied high-frequency field is responsible for the existence of the charge density Σ and this charge density also undergoes the displacement with velocity $\mathbf{v}_d$. If we had not neglected the bulk density perturbation with respect to the surface perturbation when $\beta\neq 0$, the axial current would have been multiplied by a factor $[1+O(\beta b/\lambda_0)]$. As $\mathbf{v}_d$ only intervenes in the expression of the scattered fields through $\mathbf{K}$, this means that the final expressions for G_n and F_n [see Eqs. (27) and (28)], which are proportional to v_d, would have been multiplied by a factor $[1+O(\beta b/\lambda_0)]$. This last remark fully justifies the procedure followed and the approximation made.

Equation (9) leads then to

$$(H_{Z2})_{r=b}=(H_{Z1})_{r=b}, \tag{16}$$

$$(H_{\theta 2})_{r=b}=(H_{\theta 1})_{r=b}+\left[\frac{(\boldsymbol{\sigma}\cdot\mathbf{E}_1)\cdot\mathbf{1}_r}{-i\omega}\right]_{r=b}v_d. \tag{17}$$

C. Scattered Field

The problem studied is the scattering of a plane homogeneous wave by a cylindrical plasma column with glass wall placed in vacuum (Fig. 1). Equation (4) can be written in the plasma as $\text{curl}\mathbf{H}=-i\omega\boldsymbol{\epsilon}_p\cdot\mathbf{E}$ with $\boldsymbol{\epsilon}_p$ as defined in (15). The solutions of Maxwell's equations in this medium will therefore have the same forms as when $\mathbf{v}_d=0$. It is only the surface condition (17) between plasma and dielectric, where $\mathbf{v}_d$ intervenes, which is different.

It was seen previously[16(a)] that the anisotropy does not couple the cross-polarized $\mathbf{H}$ mode to the cross-polarized $\mathbf{E}$ mode when $\mathbf{B}_0$ is axial. Here, however, the coupling occurs through the boundary condition (17). The solutions corresponding to the TE mode and the TM mode in the plasma are deduced from H_{Z1} and E_{Z1}, respectively, which each satisfy a Helmholtz equation. Noting for simplicity

$$\boldsymbol{\epsilon}_p^{-1}=\begin{vmatrix} M & iK & 0 \\ -iK & M & 0 \\ 0 & 0 & M_3 \end{vmatrix}, \tag{18}$$

with

$$M=\frac{1}{\epsilon_0}\frac{1-\Omega^2-\beta^2}{(1-\Omega^2)^2-\beta^2}, \qquad M_3=\frac{1}{\epsilon_0(1-\Omega^2)},$$

$$K=\frac{-\Omega^2\beta}{\epsilon_0[(1-\Omega^2)^2-\beta^2]}, \qquad \Omega^2=\omega_e^2/\omega^2;$$

the solutions in medium 1, which are bounded on the axis, are

$$H_{Z1}=\sum_{n=0}^{\infty} J_n(k_p r)[A_n' \cos n\theta+B_n' \sin n\theta], \tag{19}$$

$$E_{Z1}=\sum_{n=0}^{\infty} J_n(k_{p0} r)[A_n{}^{*\prime} \cos n\theta+B_n{}^{*\prime} \sin n\theta], \tag{20}$$

with $k_p{}^2=\omega^2\mu_0/M$ and $k^2{}_{p_0}=\omega^2\mu_0/M_3$. In medium 2 one has

$$H_{Z2}=\sum_{n=0}^{\infty}[M_n' J_n(k_g r)+L_n' N_n(k_g r)]\cos n\theta + \sum_{n=0}^{\infty}[T_n' J_n(k_g r)+U_n' N_n(k_g r)]\sin n\theta, \tag{21}$$

with $k_g=\omega(\epsilon_g\mu_0)^{1/2}$ and ϵ_g being the permittivity of glass. One has a similar expression for E_{Z2}.

In medium 3, both the incoming and the scattered field are present. The incoming field is characterized by an $H_{Z\,\mathrm{inc}}$ of unit amplitude

$$H_{Z\,\mathrm{inc}}=e^{ik_0 r\cos\theta}=\sum_{n=0}^{\infty}\epsilon_n i^n J_n(k_0 r)\cos n\theta, \tag{22}$$

where ϵ_n is Neumann's factor. The two modes of the scattered field are characterized by

$$H_{Z\mathrm{sc}}=\sum_{n=0}^{\infty}[J_n(k_0 r)+iN_n(k_0 r)]\times[C_n' \cos n\theta+D_n' \sin n\theta], \tag{23}$$

$$E_{Z\mathrm{sc}}=\sum_{n=0}^{\infty}[J_n(k_0 r)+iN_n(k_0 r)]\times[F_n' \cos n\theta+G_n' \sin n\theta]. \tag{24}$$

We now state the boundary conditions (9) and (11) at the two interfaces after having expressed E_r and E_θ as a function of H_Z, and, H_θ as a function of E_Z. This leads to a linear system of 16 equations for each angular mode n and the solution of this system gives the different coefficients A_n', B_n', etc. In this way one finds transcendental expressions for the coefficients C_n', D_n', F_n', and G_n' of $H_{Z\mathrm{sc}}$ and $E_{Z\mathrm{sc}}$ as a function of Ω^2. For $r=a$ and $r=b$ the arguments of the cylindrical functions corresponding to a typical experimental set-up are small so that these functions can be replaced by their asymptotic expressions

$$J_n(kr)\cong\frac{1}{n!}\left(\frac{kr}{2}\right)^n; \quad N_n(kr)\cong-\frac{(n-1)!}{\pi}\left(\frac{2}{kr}\right)^n, \quad \text{when } n\neq 0. \tag{25}$$

$J_n(kr)$ is also neglected with respect to $N_n(kr)$ in (23) and (24). In this approximation algebraical expressions for the coefficients as functions of Ω^2 are obtained. To do this conveniently the following unprimed coefficients are defined as functions of the primed ones:

$$\{A_n,B_n,M_n,T_n\}=\frac{1}{n!}\left(\frac{k}{2}\right)^n\{A_n',B_n',M_n',T_n'\}; \qquad \{L_n,U_n\}=-\frac{(n-1)!}{\pi}\left(\frac{2}{k}\right)^n\{L_n',U_n'\},$$
$$\{C_n,D_n,F_n,G_n\}=-i\left(\frac{2}{k}\right)^n\frac{(n-1)!}{\pi}\{C_n',D_n',F_n',G_n'\}; \qquad \mathcal{E}_n=\frac{2}{n!}\left(\frac{ik}{2}\right)^n. \tag{26}$$

The formulas obtained for C_n and D_n (TE mode) are, of course, identical to those obtained with $\mathbf{v}_d=0$ [Eq. (41) and (42) of Ref. 16(a)]. In this reference the interested reader will find the details of the calculation on the boundary conditions for this TE mode.

For the TM mode, the scattered field ($n\neq 0$) is characterized by

$$G_n=2v_d\mu_0\epsilon_0\epsilon_g\mathcal{E}_n \times\left\{\frac{[\epsilon_0 K_p P_n+\epsilon_g Q_n(K_p-\beta^2)/(K_p-\beta^2/K_p)]K_p(K_p-1)/(K_p-\beta^2/K_p)+\beta^2\epsilon_g Q_n[\Omega^2/(K_p-\beta^2/K_p)]^2}{[\epsilon_0 K_p P_n+\epsilon_g Q_n(K_p-\beta^2)/(K_p-\beta^2/K_p)]^2+[\beta\epsilon_g Q_n\Omega^2/(K_p-\beta^2/K_p)]^2}\right\}, \tag{27}$$

$$F_n=i2\beta v_d\mu_0\epsilon_0\epsilon_g\mathcal{E}_n\Omega^2/(K_p-\beta^2/K_p) \times\left\{\frac{\epsilon_g Q_n K_p(K_p-1)/(K_p-\beta^2/K_p)+[\epsilon_0 K_p P_n+\epsilon_g Q_n(K_p-\beta^2)/(K_p-\beta^2/K_p)]}{[\epsilon_0 K_p P_n+\epsilon_g Q_n(K_p-\beta^2)/(K_p-\beta^2/K_p)]^2+[\beta\epsilon_g Q_n\Omega^2/(K_p-\beta^2/K_p)]^2}\right\}, \tag{28}$$

with $K_p=1-\Omega^2$ and

$$\begin{pmatrix} P_n \\ Q_n \end{pmatrix} = \epsilon_0(b^{-2n} \mp c^{-2n}) + \epsilon_g(b^{-2n} \pm c^{-2n}).$$

It can be shown that for $|kr| \ll 1$ the contribution from the $n=0$ terms is zero.[21]

The physical meaning of (27) and (28) is clear. For each angular multipole n, the axial drift velocity $\mathbf{v}_d$ couples a scattered cross-polarized $\mathbf{H}$ field to the scattered cross-polarized $\mathbf{E}$ field excited by the plane incoming wave ($\mathbf{E}_{\text{inc}} \perp$ axis). The two resonances of the TM mode (which degenerate to a single one when $\beta=0$) are given by the poles of (27) and (28); these poles are identical to those of the TE mode. The two resonances occur for

$$\Omega_n^2 = \left\{1 + \frac{\epsilon_g}{\epsilon_0}\left|\frac{Q_n}{P_n}\right|\right\}, \quad (1 \pm \beta). \tag{29}$$

The resonances are characterized by infinite values of G_n and F_n because approximation (25) corresponds to neglecting radiation damping; this is the quasistatic approximation. It should be carefully noted that when $\beta=0$, F_n is equal to zero. The picture is then remarkably simple: the incombing cross-polarized $\mathbf{E}$ field in $\cos n\theta$ induces, through $\mathbf{v}_d$, an axial $\mathbf{E}_{Z\text{sc}}$ with a $\sin n\theta$ dependence.

3. COMPARISON WITH EXPERIMENTAL DATA

The axial scattered electric field $E_{Z\text{sc}}$ can be easily observed experimentally because it can be separated from the incoming field (the planes of polarization are crossed). Figure 2 shows the plasma column irradiated by an open waveguide acting as antenna ($\omega/2\pi=2.7$ GHz). The receiving antenna is constituted by a waveguide of decreasing height in order to better localize the field measured, and it can be oriented along different values of θ. The two antennas are carefully oriented (polarization planes exactly perpendicular) so that, in the absence of plasma, the receiving antenna picks up no signal. The remainder of the experimental set-up has been described previously.[4] Let us recall that the detection is strictly linear and that the oscillographic records give the amplitude of the field measured as a

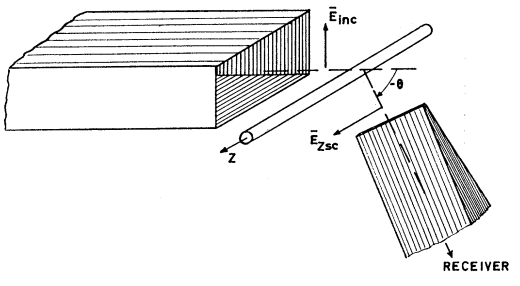

FIG. 2. Experimental setup with open wave guide irradiating plasma column and with receiving waveguide.

[21] A. M. Messiaen, D. Appl. Sc. dissertation, University of Brussels, 1963 (unpublished).

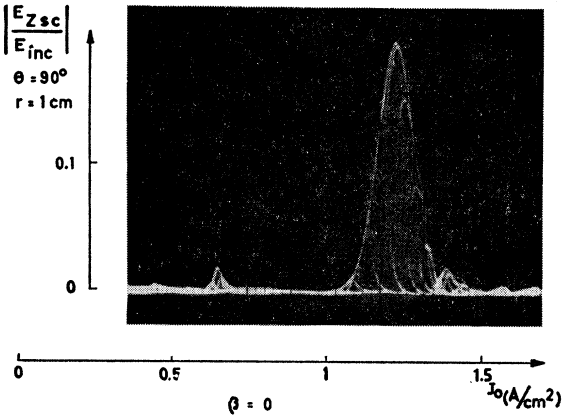

FIG. 3. $|E_{Z\text{sc}}/E_{\text{inc}}|$ as a function of discharge current density J_0 ($\propto \omega_e^2$) with no steady magnetic field ($\beta=0$).

function of the discharge current density J_0 ($\propto \omega_e^2$) in the plasma column. This plasma is obtained in the positive column of a low-pressure Hg discharge (pressure of neutrals: 2.10^{-3} Torr; $b=0.38$ cm; $c=0.527$ cm). The steady magnetic field is created by Helmholtz coils. The $n=1$ angular mode is the only one appreciably excited and we will consider it only. Figure 3 shows the main resonance for $\theta=90°$ and $\beta=0$. The $\sin\theta$ dependence of this mode has been carefully checked. The high-frequency signal is modulated to 100% and the lower horizontal line corresponds to zero incoming field. It is clear that the coupling between the TE mode and the TM mode is appreciable only near the resonance and that this coupling is null when $\omega_e \to 0$. The secondary or temperature resonances[7,10] appearing to the left are not included in our cold plasma approach, but they are, of course, also coupled by $\mathbf{v}_d$. Many precautions have been taken to ascertain that the effect observed is not due to defects in the experimental set-up. Striking experiments reported at the end of this section demonstrate this. It was seen that evanescent modes were not transmitted from the antenna to the receiver, that slight variations of the angles $(\mathbf{S},\mathbf{u}_Z)$ and $(\mathbf{E}_{\text{inc}},\mathbf{u}_Z)$ did not affect the results in a critical fashion, that reflecting obstacles placed perpendicularly to the column had but small effects, and that the phenomenon was a linear function of $|\mathbf{E}_{\text{inc}}|$. No wave propagation along the cylinder axis or standing waves have been observed.

Typical results are given for $\theta=90°$ and $\theta=0°$ as a function of β in Figs. 4 and 5. Because of the Helmholtz coils, it has proved impossible to annul completely $E_{Z\text{sc}}$ when $\omega_e=0$ as was successfully done without Helmholtz coils in Fig. 3. Theoretical results corresponding to $\beta=0.15$ and obtained through computation on Eqs. (27) and (28) with experimental values of the parameters ($n=1$, $v_d=3\times10^7$ cm sec^{-1})[22] are given in

[22] The value of v_d is calculated from the position of the main resonance in back scattering [Ref. 9 (a)]. This value agrees with that computed from the determination of the mobility after using Davison's relation (Refs. 21, 23).

[23] P. Davidson, Proc. Phys. Soc. (London) **B67**, 159 (1954).

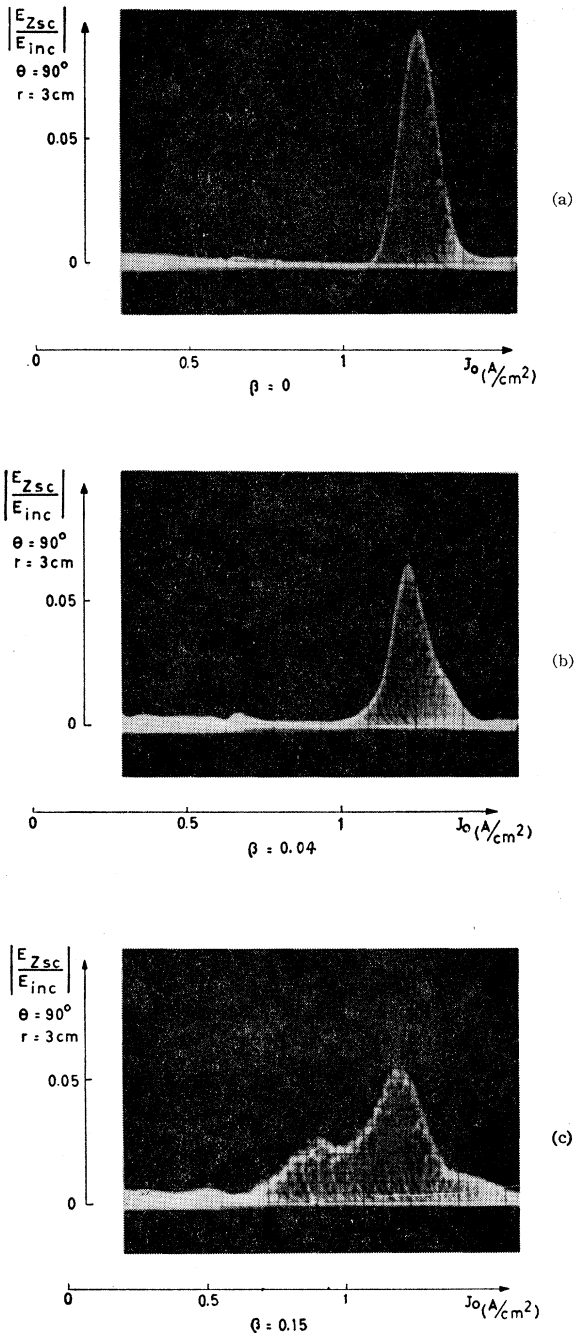

FIG. 4. Oscillograms giving $|E_{Zsc}/E_{inc}|$ as a function of discharge current density J_0 for $\theta=90°$ and different values of β.

Figs. 6 and 7. As predicted by theory, it is seen that when $\beta=0$, there is one main resonance of E_{Zsc} which has a $\sin\theta$ dependence [Figs. 4(a) and 5(a)]; when $\beta\neq 0$, there appears another component of E_{Zsc} which has a $\cos\theta$ dependence and it increases linearly with β [Fig. 5(a) and 5(b)]. Furthermore, the resonances split [Figs. 4(c) and 5(c); the supplementary resonances to the right of 5(c) are due to multipoles $n>1$[15,16(b)]], and the values of J_0 which correspond to them are practically identical to those found for the resonances of $E_{\theta sc}$ (see Refs. 15 and 16 for the comparison between theory and experiments concerning the position of these resonances).

The amplitude of the observed phenomenon is also compared to that of the predicted one. We did this for

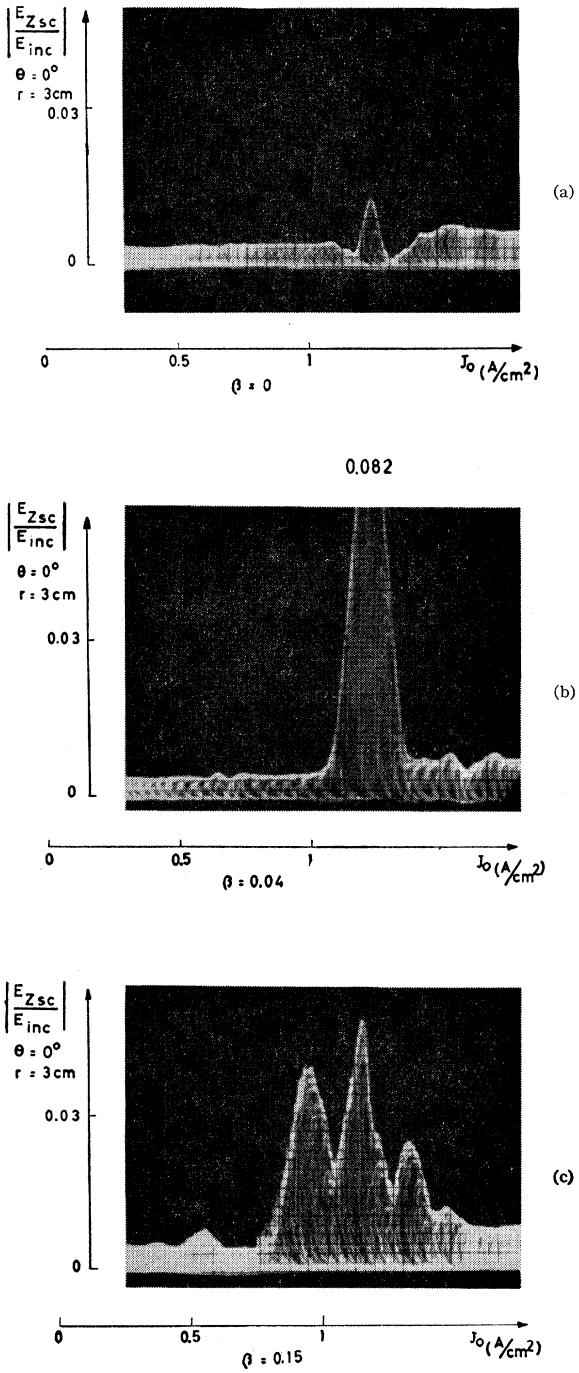

FIG. 5. Oscillograms giving $|E_{Zsc}/E_{inc}|$ as a function of discharge current density J_0 for $\theta=0°$ and different values of β.

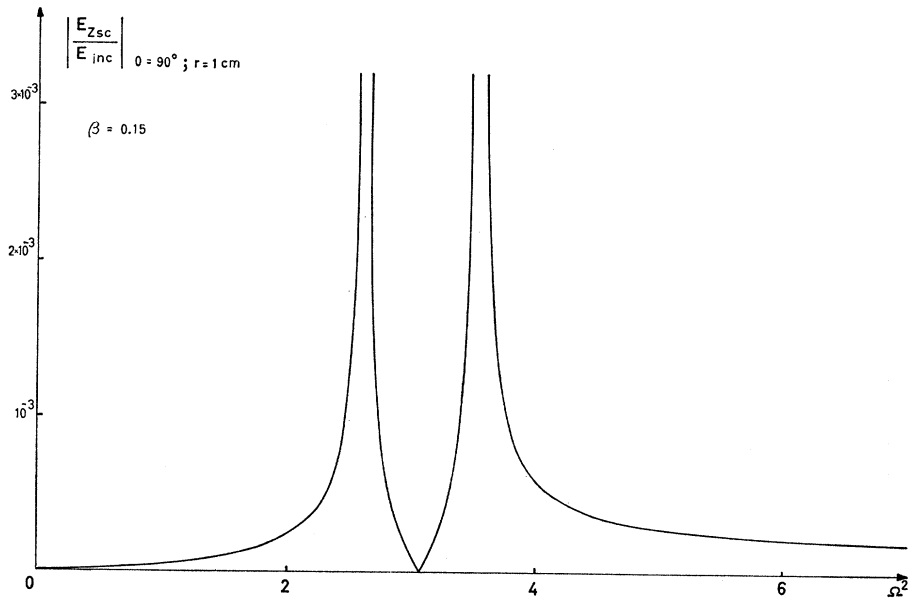

FIG. 6. Theoretical curve of $|E_{Zsc}/E_{inc}|$ as a function of Ω^2 for $\theta=90°$ and $\beta=0.15$.

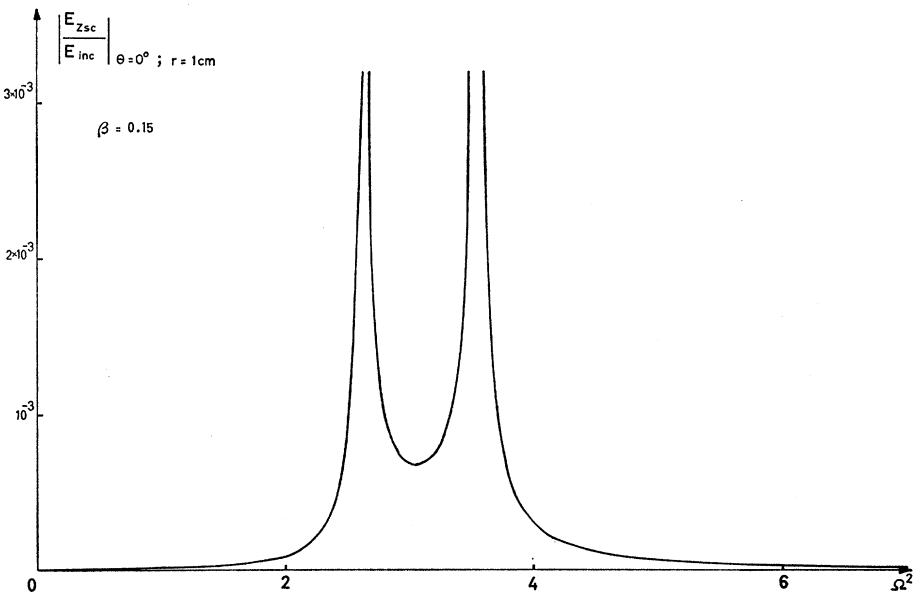

FIG. 7. Theoretical curve of $|E_{Zsc}/E_{inc}|$ as a function of Ω^2 for $\theta=0°$ and $\beta=0.15$.

$\beta=0$. To obtain the amplitude of the resonance theoretically, we consider only the radiation damping which is preponderant in the experimental case considered.[5,21] $J_n(k_0r)$ must not be neglected then with respect to $N_n(k_0r)$ in (23) and (24) when expressing the boundary conditions. $|G_1|$ remains then finite at resonance and is given by

$$|G_1|_{\max}=\left|\frac{8\mu_0 v_d \epsilon_g \epsilon_0 \Omega^2 \mathcal{E}_1}{\pi k_0^2 c^2[\epsilon_p R_1+\epsilon_g S_1]}\right|, \qquad (30)$$

with

$$\binom{R_1}{S_1}=\epsilon_0(b^{-2}\mp c^{-2})-\epsilon_g(b^{-2}\pm c^{-2}).$$

The maximum theoretical value of $|E_{Zsc}|$ with respect to $|E_{inc}|$ is given in Fig. 8 for $r=1$ cm. The maximum experimental value of $|E_{Zsc}/E_{inc}|$ was obtained through measuring $|\mathbf{E}_{inc}|$ by placing the receiving waveguide at $\theta=0°$ and parallel to the emitting waveguide. These theoretical and experimental values are listed in Table I for $r=1$ cm. It is seen that the effect observed is at

TABLE I. $|E_{Zsc\,max}/E_{inc}|_{r=1\,cm}$

Theoretical	Experimental
0.3×10^{-2}	16×10^{-2} to 30×10^{-2}

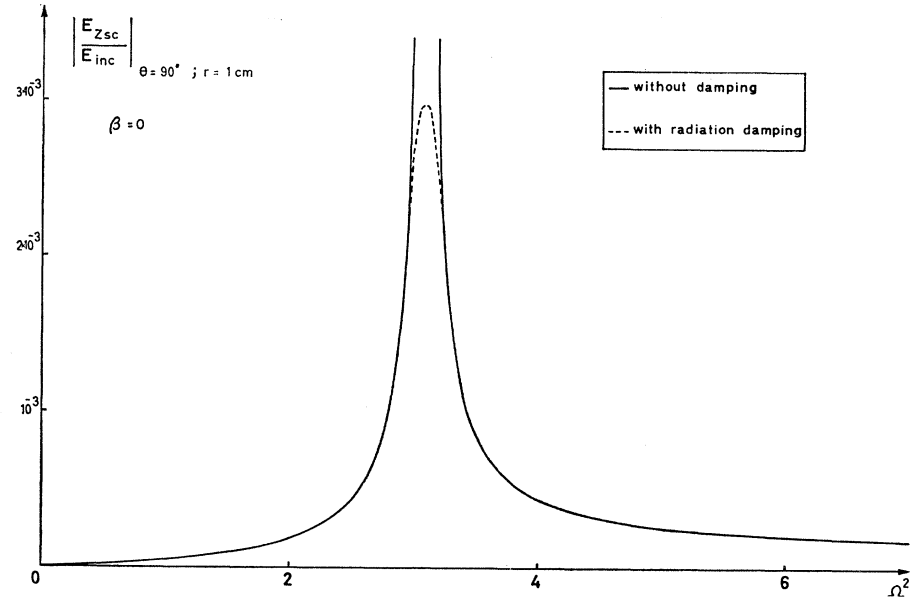

FIG. 8. Theoretical curve of $|E_{Zsc}/E_{inc}|$ as a function of $\Omega^2=\omega_e^2/\omega^2$.

least one order of magnitude higher than the predicted one. This discrepancy does not seem, at first sight, to be explainable by a perturbation in the scattered field due to the presence of the receiving antenna or by the approximations done in the theory. Indeed, when the inhomogeneity of the plasma is taken into account in simpler cases, the influence on the cold plasma resonance remains small and the influence of nonzero temperature T_e on this same resonance is also small.[7,10] These two effects should, however, be investigated in this particular instance. On the other hand, we have verified that the amplitude of E_{Zsc} does vary as a function of r like $|J_1(k_0r)+iN_1(k_0r)|$ in the neighborhood of the column. In this connection, it must be mentioned that this is one of the first comparisons of the *absolute* magnitude of an experimental amplitude with respect to a theoretical one in a scattering experiment. This comparison, although rather delicate, is facilitated by our linear detecting system and by the cross-polarization of E_Z with respect to the incoming field. The other instance in which amplitudes have been compared is in Stern and Tzoar's experiments on nonlinear effects at plasma resonance.[24,25] It should also be remarked that although the resonant frequencies of the secondary or temperature spectrum are now well understood,[7,10,11] the amplitudes of the secondary resonances—when compared to the main one—are much greater in mercury than in other gases,[26,27] and this difference has not been explained so far.

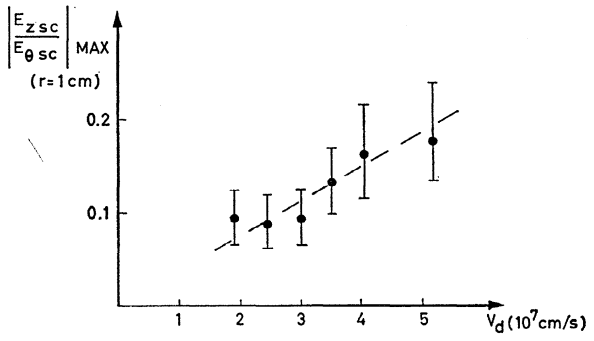

FIG. 9. Experimental $|E_{Zsc}/E_{\theta sc}|_{max}$ as a function of v_d.

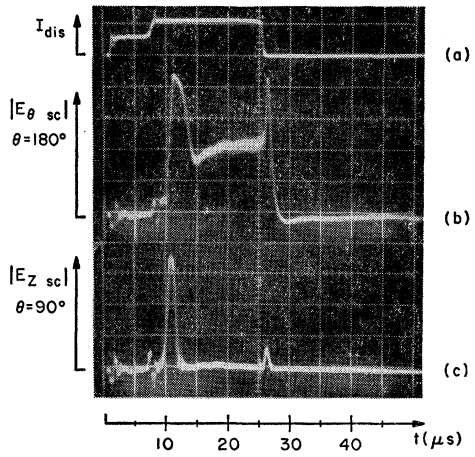

FIG. 10. (a) Discharge current as a function of time t (1 vertical div. = 1A); (b) E_θ at 180° (back-scattered field) versus t (arbitrary linear vertical scale); resonance peak to the left occurs during the electron density rise and peak to the right occurs during the density decay; (c) E_Z at $\theta=90°$ versus t ($E_{inc}=25$ vertical div.); peak to the left occurs when $v_d\neq 0$ and peak to the right occurs when v_d is practically zero ($\nu_c=3.5\times10^7$ sec^{-1}).

[24] R. A. Stern, Phys. Rev. Letters **14**, 538 (1965).
[25] R. A. Stern and N. Tzoar, Phys. Rev. Letters **15**, 485 (1965).
[26] A. Messiaen, Physica (L) **29**, 1117 (1963).
[27] R. A. Stern, J. Appl. Phys. **34**, 2562 (1963).

The drift velocity can be varied, but only within certain limits, in the discharge tube by changing the mercury vapor pressure. Such an experiment is not as precise as the previous ones since other parameters vary also. The results are shown on Fig. 9, where $E_{Z\mathrm{sc}}$ is compared to $E_{\theta\mathrm{sc}}$ rather than to E_{inc} in order to exclude the collision effects which become greater at higher pressure. Again the value of v_d is calculated from the position of the main resonance in back scattering. The discharge becomes very unstable for pressures of the order of 5×10^{-4} Torr (high values of v_d) and the dispersion of the results is high. The results shown on Fig. 9 indicate that $|E_{Z\mathrm{sc}}|_{\max}$ roughly increases with v_d but they cannot be precise enough to demonstrate a linear dependence between $|E_{Z\mathrm{sc}}|_{\max}$ and v_d.

An afterglow experiment shows directly the influence of v_d on the magnitude of $E_{Z\mathrm{sc}}$. The plasma is created by a current pulse in the discharge tube as shown on Fig. 10(a). During the ionizing pulse, the electron density rises to a maximum value and the density decreases then as a function of time (time scale: 1 horizontal division corresponds to 5 μsec). During the current pulse, the plasma possesses a drift velocity which disappears very rapidly as the current drops, since the collision frequency ν_c is approximately 3.5×10^7 sec^{-1}. The incident electromagnetic wave is shone on the column as formerly. Figure 10(b) displays to the left the main or cold plasma resonance in reflection (E_θ for $\theta=180°$) during the rise of the plasma density, while the resonance peak to the right is obtained during the decay of the density at the time when this density corresponds to that for the main resonance. The fact that the resonant amplitudes are the same in both cases shows that—except for the drift velocity which does not influence E_θ—the global properties (radial density distribution, etc.) of the plasma do not differ significantly. Figure 10(c) displays E_Z as a function of t. One observes, as expected, a resonance peak on the left which occurs at the same time (density) as the E_θ peak; it is characterized by $|E_{Z\mathrm{sc}}/E_{\mathrm{inc}}|=0.17$. A second and much smaller resonance peak, occurring again in coincidence with the E_θ peak, is seen to the right; it is characterized by $|E_{Z\mathrm{sc}}/E_{\mathrm{inc}}|=0.03$. As demonstrated by Fig. 10(b), the essential difference is that v_d is present in the first instance and that the collisions have considerably reduced it in the second; Fig. 10(c) shows therefore conclusively that $E_{Z\mathrm{sc}}$ is linked to the existence of $\mathbf{v}_d$.

Another experiment which also shows the direct connection between v_d and $E_{Z\mathrm{sc}}$ is the following: the direction of $\mathbf{v}_d$ is reversed by exactly rotating the tube by an angle of 180° around the vertical. The amplitude and the phase of a reference signal E_{ref} is adjusted in such a way that the combined signal $E_{\mathrm{ref}}+E_{Z\mathrm{sc}}$ is equal to zero at resonance when it is displayed as a function of J_0 on an oscilloscope. When $\mathbf{v}_d$ is reversed one observes $2|E_{\mathrm{ref}}|$ at resonance; this shows that the sign of $E_{Z\mathrm{sc}}$ is also reversed as predicted by Eq. (27).

4. CONCLUSIONS

We wish to draw attention to the similarity existing between the phenomenon described here and the classic static experiments of Roentgen and Eichenwald.[17–19] In the latter experiments, a dielectric is placed in the uniform electrostatic field $\mathbf{E}$ of a plane condenser, and is displaced parallel to the plates with a velocity $\mathbf{v}$. The polarization charges are displaced with this velocity and create a magnetostatic field perpendicular to both $\mathbf{E}$ and $\mathbf{v}$. It is therefore seen that the phenomenon described in this paper is, in a sense, the high-frequency plasma analog of the effects due to the Roentgen-Eichenwald current.

The drift velocity effect is, of course, a direct consequence of the covariance of Maxwell's equations with respect to the Lorentz transformations of special relativity. This explains the reason why the axially moving charges of the whole plasma, in the presence of a TE excitation, thus give rise to TM fields. In the cold-plasma limit, however, the structure of the plasma equations imply, when $\mathbf{B}_0=B_0\mathbf{1}_Z$, $\partial/\partial Z\equiv0$ and $\beta b/\lambda_0\ll1$, the description of the plasma by high-frequency surface charges of polarization, and we then obtain the high-frequency analog of the Roentgen-Eichenwald current.

To conclude, we wish again to stress that the position of the resonances and the angular distribution of the axial electric field scattered by a mercury plasma are very correctly explained by our theoretical approach which uses a cold-uniform-plasma model to predict a new effect, namely the existence of an $E_{Z\mathrm{sc}}$ component when there is an axial drift velocity. The observed amplitude of the effect is nevertheless at least an order of magnitude greater than the one predicted by this model. An afterglow experiment and a phase-flipping experiment show, however, that the observed E_Z is linked to the existence of v_d.

ACKNOWLEDGMENTS

We wish to thank Professor R. W. Gould and Professor C. H. Papas of the California Institute of Technology and Professor R. Balescu of the University of Brussels for carefully reading the manuscript and for interesting discussion of the results. One of the authors (P.V.) is indebted to the U. S. Air Force Office of Scientific Research for partial support of this research.

APPENDIX A: ROLE OF THE SELF-MAGNETIC FIELD

We consider the case where the applied magnetic induction $\mathbf{B}_0$ is zero. In Eq. (1) we only include the self steady magnetic induction which is due to the drift velocity of the plasma: $B_{0T}=B_{0\theta}=\frac{1}{2}\mu_0 J_0 r$. All that has been said in Secs. 2A and 2B remains unchanged with the exception of the expression for σ and thus for ε_p. We solve Maxwell's equations in medium 1 and match the boundary conditions. We look for a solution to first order in $\beta_\theta=eB_{0\theta}/m\omega$ which can be obtained from the

following equations[15,16(a)]

$$\nabla\times\varepsilon^{-1}\nabla\times\mathbf{H}=\omega^2\mu_0\mathbf{H},\qquad \mathrm{div}\mathbf{H}=0,\quad \partial/\partial Z=0, \tag{A1}$$

with

$$\varepsilon^{-1}=\begin{vmatrix} M & 0 & iK_\theta \\ 0 & M & 0 \\ -iK_\theta & 0 & M_3 \end{vmatrix} \tag{A2}$$

where

$$M\cong M_3=1/\epsilon_0(1-\Omega^2);\quad K_\theta=(\beta_\theta/\epsilon_0)\Omega^2/(1-\Omega^2)^2.$$

(A1) leads to the system of equations:

$$[\nabla_T^2+k_{p0}^2]H_Z-i\frac{K_\theta}{M}k_{p0}^2\frac{1}{r}\frac{\partial\phi}{\partial\theta}=0, \tag{A3}$$

$$[\nabla_T^2+k_{p0}^2]\phi-i\frac{K_\theta}{M}\frac{1}{r}\frac{\partial H_Z}{\partial\theta}=0, \tag{A4}$$

in which ϕ is the function characterizing the cross-polarized $\mathbf{H}$ mode such that

$$H_r=-(1/r)\partial\phi/\partial\theta;\quad H_\theta=\partial\phi/\partial r. \tag{A5}$$

Eliminating ϕ or H_Z between (A3) and (A4) and taking into account the fact that K_θ/r is a constant, one finds a fourth-order differential equation of the form

$$\left\{(\nabla_T^2+k_{p0}^2)+i\tau\frac{\partial}{\partial\theta}\right\}\times\left\{(\nabla_T^2+k_{p0}^2)-i\tau\frac{\partial}{\partial\theta}\right\}\begin{Bmatrix}H_Z\\ \phi\end{Bmatrix}=0, \tag{A6}$$

with $\tau=K_\theta k_{p0}/rM$. The solution of (A6) which is bounded on the axis is

$$\begin{aligned} H_Z&=\sum_{n=-\infty}^{\infty}\{a_{1n}J_n(r[k_{p0}^2-n\tau]^{1/2})+a_{2n}J_n(r[k_{p0}^2+n\tau]^{1/2})\}e^{in\theta},\\ \phi&=\sum_{n=-\infty}^{\infty}\{b_{1n}J_n(r[k_{p0}^2-n\tau]^{1/2})+b_{2n}J_n(r[k_{p0}^2+n\tau]^{1/2})\}e^{in\theta}, \end{aligned} \tag{A7}$$

where the a's and the b's are constants. H_Z and ϕ, given by (A7), are not independent as they must satisfy (A3) and (A4). This imposes $a_{1n}=-k_{p0}b_{1n}$; $a_{2n}=k_{p0}b_{2n}$. We regroup the terms of (A7) to bring out the $\sin\theta$ and $\cos\theta$ dependence and in so doing we use the fact that $k_{p0}r\ll1$ and $\tau r\ll1$ in our experimental set-up. Approximating the J_n's by the first term of their power series, we obtain to first order in β_θ, i.e., in τ

$$H_Z=\sum_{n=0}^{\infty}r^n\left\{\left(A_n+\frac{i}{2}\frac{n^2\tau}{k_{p0}^2}\beta_n\right)\cos n\theta+\left(B_n+\frac{i}{2}\frac{n^2\tau}{k_{p0}^2}\alpha_n\right)\sin n\theta\right\}, \tag{A8}$$

$$\phi=\sum_{n=0}^{\infty}\frac{r^n}{k_{p0}}\left\{\left(-\beta_n+\frac{i}{2}\frac{n^2\tau}{k_{p0}^2}A_n\right)\sin\theta+\left(\alpha_n-\frac{i}{2}\frac{n^2\tau}{k_{p0}^2}B_n\right)\cos n\theta\right\}, \tag{A9}$$

where α_n, β_n, A_n, and B_n are constants. The components of $\mathbf{E}$ and $\mathbf{H}$ are easily derived from H_Z and ϕ. It is seen that in the plasma the $\cos n\theta$ terms of one mode (e.g., the TE mode) are coupled to the $\sin n\theta$ terms of the other mode (e.g., the TM mode).

We must now express the boundary conditions (9) and (11). We do this first by putting $K=0$ in order to study only the effect of $B_{0\theta}$. This leads to

$$\beta_n=\tfrac{1}{2}i(n^2\tau/k_{p0}^2)A_n\quad\text{and}\quad\alpha_n=\tfrac{1}{2}i(n^2\tau/k_{p0}^2)B_n. \tag{A10}$$

This means that the boundary conditions of the problem do not permit the excitation of the TM mode through the intrinsic coupling in the plasma when the solutions are expressed by (A8) and (A9), i.e., to first order in β_θ.

We then compute $\mathbf{K}$ using (14) and take simultaneously into account the existence of $\mathbf{K}$ and $\mathbf{B}_{0\theta}$. If the approximation $|k_{0p}^2r^2|\ll1$—which is the approximation used consistently throughout the paper—is made, the results obtained for $E_{Z\mathrm{sc}}$ are identical to those obtained by neglecting $\mathbf{B}_{0\theta}$.

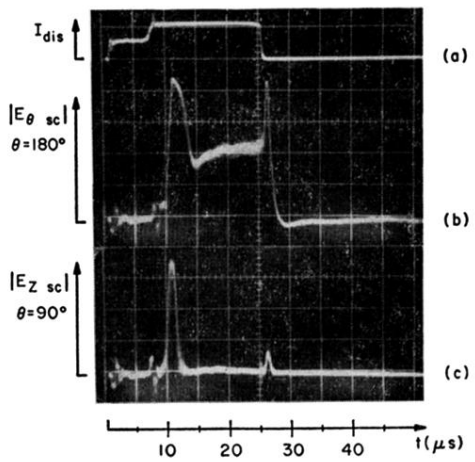

FIG. 10. (a) Discharge current as a function of time t (1 vertical div. = 1A); (b) E_θ at 180° (back-scattered field) versus t (arbitrary linear vertical scale); resonance peak to the left occurs during the electron density rise and peak to the right occurs during the density decay; (c) E_Z at $\theta=90°$ versus t ($E_{\text{inc}}=25$ vertical div.); peak to the left occurs when $v_d\neq 0$ and peak to the right occurs when v_d is practically zero ($\nu_c=3.5\times 10^7$ sec^{-1}).

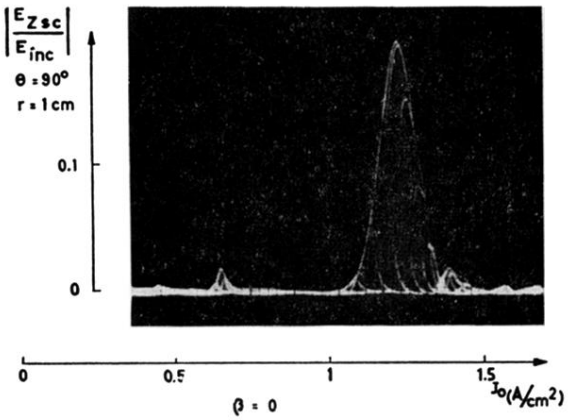

FIG. 3. $|E_{Z\mathrm{sc}}/E_{\mathrm{inc}}|$ as a function of discharge current density J_0 ($\propto \omega_e^2$) with no steady magnetic field ($\beta = 0$).

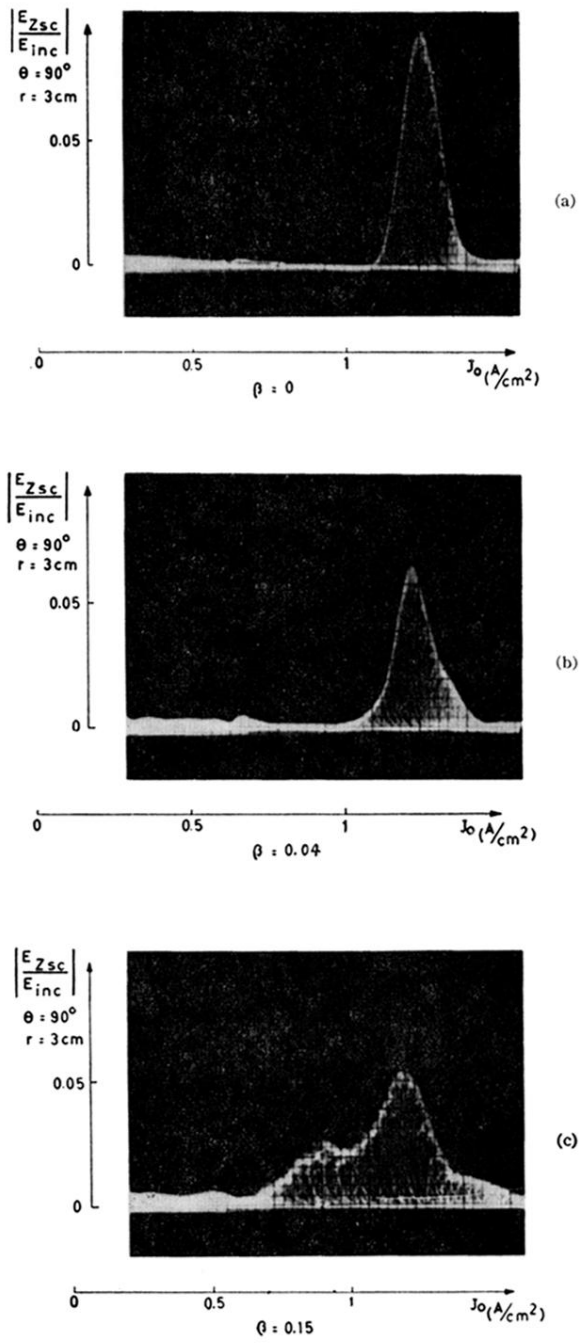

FIG. 4. Oscillograms giving $|E_{Zsc}/E_{inc}|$ as a function of discharge current density J_0 for $\theta=90°$ and different values of β.

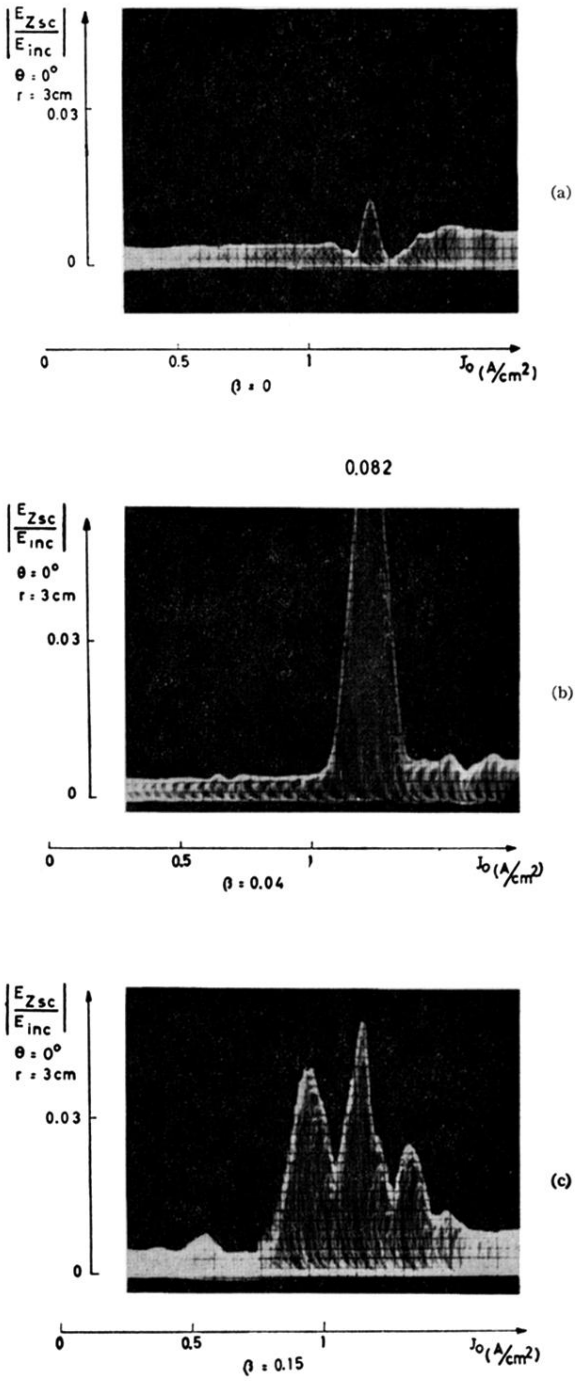

FIG. 5. Oscillograms giving $|E_{Zsc}/E_{inc}|$ as a function of discharge current density J_0 for $\theta=0°$ and different values of β.